



HAL
open science

A non-human primate model of stroke reproducing endovascular thrombectomy and allowing long-term imaging and neurological read-outs

Justine Debatisse, Océane Wateau, Tae-Hee Cho, Nicolas Costes, Inés Mérida, Christelle Léon, Jean-Baptiste Langlois, Fabrice Taborik, Michaël Verset, Karine Portier, et al.

► To cite this version:

Justine Debatisse, Océane Wateau, Tae-Hee Cho, Nicolas Costes, Inés Mérida, et al.. A non-human primate model of stroke reproducing endovascular thrombectomy and allowing long-term imaging and neurological read-outs. *Journal of Cerebral Blood Flow and Metabolism*, 2021, 41 (4), pp.745-760. 10.1177/0271678x20921310 . hal-02901927

HAL Id: hal-02901927

<https://hal.science/hal-02901927v1>

Submitted on 24 Jan 2025



HAL is a multi-disciplinary open access archive for the deposit and dissemination of scientific research documents, whether they are published or not. The documents may come from teaching and research institutions in France or abroad, or from public or private research centers.

L'archive ouverte pluridisciplinaire **HAL**, est destinée au dépôt et à la diffusion de documents scientifiques de niveau recherche, publiés ou non, émanant des établissements d'enseignement et de recherche français ou étrangers, des laboratoires publics ou privés.



Distributed under a Creative Commons Attribution - NonCommercial 4.0 International License

A non-human primate model of stroke reproducing endovascular thrombectomy and allowing long-term imaging and neurological read-outs

Justine Debatisse^{1,2,*} , Océane Wateau^{3,4,*}, Tae-Hee Cho^{1,5,6}, Nicolas Costes⁷, Inés Mérida⁷, Christelle Léon¹, Jean-Baptiste Langlois⁷, Fabrice Taborik³, Michaël Verset³, Karine Portier¹ , Mohamed Aggour¹, Thomas Troalen², Marjorie Villien⁷, Nikolaos Makris⁵, Christian Tourvieille⁷, Didier Le Bars^{6,7}, Sophie Lancelot^{6,7}, Joachim Confais³, Adrien Oudotte⁶, Norbert Nighoghossian^{1,6}, Michel Ovize^{1,6}, Denis Vivien^{4,8}, Hugues Contamin³, Véronique Agin^{4,*}, Emmanuelle Canet-Soulas^{1,*} and Omer Faruk Eker^{5,6,*}

Abstract

Stroke is a devastating disease. Endovascular mechanical thrombectomy is dramatically changing the management of acute ischemic stroke, raising new challenges regarding brain outcome and opening up new avenues for brain protection. In this context, relevant experiment models are required for testing new therapies and addressing important questions about infarct progression despite successful recanalization, reversibility of ischemic lesions, blood–brain barrier disruption and reperfusion damage. Here, we developed a minimally invasive non-human primate model of cerebral ischemia (*Macaca fascicularis*) based on an endovascular transient occlusion and recanalization of the middle cerebral artery (MCA). We evaluated per-occlusion and post-recanalization impairment on PET-MRI, in addition to acute and chronic neuro-functional assessment. Voxel-based analyses between per-occlusion PET-MRI and day-7 MRI showed two different patterns of lesion evolution: “symptomatic salvaged tissue” (SST) and “asymptomatic infarcted tissue” (AIT). Extended SST was present in all cases. AIT, remote from the area at risk, represented 45% of the final lesion. This model also expresses both worsening of fine motor skills and dysexecutive behavior over the chronic post-stroke period, a result in agreement with cortical-subcortical lesions. We thus fully characterized an original translational model of ischemia–reperfusion damage after stroke, with consistent ischemia time, and thrombus retrieval for effective recanalization.

Keywords

Endovascular non-human primate stroke model, ischemia–reperfusion, neurofunctional tests, PET-MRI imaging, thrombectomy

¹Univ Lyon, CarMeN Laboratory, INSERM, INRA, INSA Lyon, Université Claude Bernard Lyon 1, Lyon, France

²Siemens-Healthcare SAS., Saint-Denis, France

³Cynbiose SAS, Marcy-L'Etoile, France

⁴Normandie Université, UNICAEN, INSERM, INSERM UMR-S 1237, “Physiopathology and Imaging of Neurological Disorders”, Institut Blood and Brain @ Caen Normandie, GIP Cyceron, Caen, France

⁵CREATIS, CNRS UMR-5220, INSERM U1206, Université Lyon 1, INSA Lyon Bât. Blaise Pascal, Villeurbanne, France

⁶Hospices Civils of Lyon, Lyon, France

⁷CERMEP – Imagerie du Vivant, Lyon, France

⁸Department of Clinical Research, Caen-Normandy Hospital, CHU Caen, Caen, France

*These authors contributed equally to this work.

Corresponding author:

Emmanuelle Canet-Soulas, Laboratoire CarMeN, Université de Lyon INSERM U.1060/Université Lyon1/INRA U. 1397/INSA Lyon/Hospices Civils Lyon U1060 CarMeN, bât. B13, Groupement Hospitalier Est 59 Boulevard Pinel, Bron 69500, France.
Email: emmanuelle.canet@univ-lyon1.fr

Introduction

Acute ischemic stroke (AIS) consecutive to large vessel occlusion (LVO) currently accounts for a significant proportion of stroke patients admitted to acute stroke units, and leads to death or disability. In AIS, time is critical: rapid recanalization (i.e. artery reopening) is mandatory. The emergence of endovascular mechanical thrombectomy (MT) has enhanced recanalization rates, which has translated into better outcomes. However, more than 50% of patients undergoing MT will remain disabled, at least in part due to a “no-reflow” phenomenon (i.e. inappropriate reperfusion despite recanalization) and other forms of ischemia–reperfusion damage. Their respective contributions and the mechanisms underlying ischemia–reperfusion injury in AIS remain unclear, but evidence points to microvascular injury secondary to LVO. Furthermore, MT is an expensive and highly specialized procedure to which only a very small minority of patients have access. This underlines the need for strategies identifying patients who may most benefit from MT thus improving the efficacy and safety of patient management.

Patient eligibility for thrombectomy is mainly based on imaging criteria, such as estimates of the infarct core and at-risk tissue (i.e. ischemic penumbra). Downstream flow may not be fully restored despite successful proximal recanalization, and further brain damage may occur; the new clinical context of MT therefore requires (i) better understanding of the mechanisms contributing to cerebral recanalization and reperfusion following fibrinolysis and MT, alone or combined; (ii) identification of adequate biological, functional and/or imaging biomarkers of treatment response; and (iii) experimental translational models to test new ischemia–reperfusion injury therapies.

Among the numerous ischemic stroke models (ISM) previously reported, the advantages of non-human primate (NHP) models are commonly agreed.¹ The ideal stroke model should be minimally invasive, reproducible with minimal variability, reversible, and above all compatible with per-occlusion and per-recanalization imaging. It should also cause minimal postoperative impairment, to ensure animal survival and allow longitudinal functional assessment.^{1–3} Most reported NHP stroke models were based on invasive surgical approaches (transorbital and/or with craniotomy) and/or permanent middle cerebral artery occlusion (MCAO) with large infarct volume and poor outcome. Furthermore, few of these models were compatible with full imaging assessment including the penumbra.^{4–10}

The goal of the present study was to develop a reversible, survivable endovascular method of inducing

ischemia–reperfusion stroke in NHP with imaging and behavioral read-outs, as close as possible to clinical observations. It was meant to enable per-occlusion evaluation of cerebral damage and penumbra, and post-occlusion follow-up. Using multiparametric voxel-based PET-MRI measurements and serial neurological assessment, we evaluated the regional regression and progression of lesions during the course of ischemia–reperfusion, and acute and chronic functional outcome. This analysis was intended to determine respective contributions to final outcome, and to identify potential translational targets of neuroprotection in the MT era.

Materials and methods

Animals

All experiments were carried out in accordance with the European Directive 2010/63/UE and ARRIVE guidelines (Animal Research: Reporting in Vivo Experiments) and approved by the Animal Welfare Body of Cynbiose and the Ethics Committee of VetAgro-Sup. The animal facility of Cynbiose is fully accredited by the Association for Assessment and Accreditation of Laboratory Animal Care (AAALAC). More details on the materials and methods can be found in the Supplemental Materials.

Animal model and stroke induction

The study included mature male cynomolgus macaques (*Macaca fascicularis*) sourced from Mauritius. In a pilot phase, intervention in seven animals allowed us to refine the endovascular MCA procedure under general anesthesia (Supplemental Materials and Methods). MCA occlusion and recanalization were achieved by deploying and retrieving non-detached endovascular microcoil, reproducibly and without any immediate perioperative complications. This innovative procedure enabled MRI imaging with minimal artifacts during occlusion and immediately after recanalization (i.e. in-bore coil retrieval). The procedure was then used for the rest of the study (Supplemental Materials and Methods).

Animals were pair-housed with free access to water and mixed diet. For stroke induction, anesthesia was induced by IM injection of ketamine (4 mg/kg; Ketamine® 1000, Virbac, France) and midazolam (1.3 mg/kg; Midazolam® 5 mg/mL, Mylan, France) and maintained throughout the procedure by sevoflurane (1%, variable depending on the animal's anesthetic depth; SevoFlo®, Abbott Laboratories, France). Fentanyl (0.04 mL/kg/h; Fentadon® 50 µg/mL, Dechra, France) was used as analgesia during the procedure.

Animals were intubated and placed on a heating mattress, connected to the monitoring equipment (SCHILLER Maglife, Switzerland) via various sensors: heart and respiratory rate, ET-CO₂, systolic, diastolic and mean arterial pressure, oxygen saturation and body temperature were monitored continuously to ensure a safe level of anesthesia.

After right common femoral artery puncture and intra-arterial navigation under fluoroscopic guidance through the aorta and the left carotid artery, a 0.017-inch microcatheter was positioned in the left MCA. After confirmation of good microcatheter positioning, a platinum framing coil (OPTIMA, Balt, Montmorency, France) was gently deployed without detachment within the superior or inferior M2 branch of the left MCA. Based on both various anatomical configurations of the MCA and its segmental distribution, the dominant M2 branch of the MCA was selected for occlusion with the aim of increasing the likelihood of obtaining a significant and evaluable infarct core. After checking successful MCAO, the catheter system was secured in position and the animal was transferred to the PET-MR scan facility for per-occlusion and per-reperfusion imaging. The coil remained undetached in position for the duration of occlusion. At the end of the MCAO time, revascularization was achieved by gently removing the coil through the femoral introducer within the PET-MRI scanner (i.e. in-bore recanalization). No heparin was administered during the whole endovascular procedure. At the end of the experiment (i.e. end of post-reperfusion imaging), hemostasis at the groin puncture point was obtained by manual compression for 20 min, followed by a compressive bandage. Buprenorphine (0.02 mg/kg, Buprecare[®] 0.3 mg/ml, Axience, France) was used as post-operative analgesic.

The PET-MRI and longitudinal neurological follow-up consisted in: (1) baseline imaging and behavioral training; (2) MCAO under general anesthesia and fluoroscopic guidance, and animal transfer from the cathlab to the PET-MRI facility; (3) per-occlusion imaging; (4) in-bore recanalization and post-recanalization imaging; (5) wake-up and clinical follow-up; and (6) day-7 and day-30 PET-MRI follow-up, together with serial neurofunctional tests (Figure 1(a)). Imaging data were acquired on the fully integrated hybrid Biograph mMR PET-MRI scanner at baseline (several weeks before the vascular procedure), per-occlusion and post-revascularization, and at 7 (D7) and 30 days (D30) after revascularization (Figure 1). The MRI protocol consisted of high-resolution T1-weighted MPRAGE, T2 fluid-attenuated inversion recovery imaging (FLAIR), 3D-DWI, 3D time-of-flight MR angiography (3D-TOF-MRA), T2/T2* multi-echo spin echo/gradient echo

(T2/T2* mapping) and a 3 min T2*-echo planar imaging (EPI) gadolinium-enhanced PWI with bolus injection of 4 mL Dotarem[®] (Guerbet, France) followed by i.v. injection of 10 ml saline (injection rate, 3 ml/s) using a power injector (MEDRAD[®], Bayer, Switzerland) (Table S1 for imaging parameters). Dynamic brain perfusion PET data were acquired over 6 min after bolus injection of radiotracer [¹⁵O]H₂O (255 ± 15 MBq) followed by i.v. injection of 10 ml saline (injection rate, 3 ml/s) using the power injector. During occlusion, the infarct core was evaluated by diffusion-weighted imaging (DWI) and the ischemic penumbra by perfusion-weighted imaging (PWI) and PET-[¹⁵O]H₂O perfusion imaging (Table S1 for acquisition parameters).

Longitudinal post-stroke functional assessment

We developed a neurological scale (Non-Human Primates Neurological Scale: NHPNS) to evaluate NHP neurological status following MCAO induction. The scale was adapted for our model from the National Institutes of Health Stroke Scale (NIHSS) used in humans and from a few scales used in NHPs.^{11,12} The neurological evaluations were quantitated as scores, with higher scores reflecting poor functional status. Of the 60 points possible, 10 were assigned to spontaneous activities (food and water intake, stereotypies, interactions between NHPs and interactions with humans), 29 to remote neurological examination (state of consciousness, posture, motor coordination and balance, movement disorder, distal and proximal limb motricity, tone), and 21 to close-up neurological examination (facial motricity, neuro-ophthalmology, upper and lower limb somesthesia). The NHPNS is described in detail in the Supplementary Table S2. Assessments were conducted by two experimented independent observers.

For evaluation of fine motor function and evolution over time, a hand dexterity task (HDT), adapted from,^{13,14} was used. Animals were required to retrieve small rewards from wells of various diameters and positions, with either the right or the left hand. Each monkey was trained on this task for at least one month pre-surgery, and then longitudinally tested over the 28-day period following the stroke. Twelve trials (six per hand) were conducted, in random order of well diameter and location, for each endpoint. Reward retrieval latency was used as a quantitative measure of hand motor performance. Further details about the test are described in the Supplemental Materials and Methods.

To assess cognitive function and long-term outcome following stroke, a delayed response task (DRT), adapted from literature,¹⁵⁻¹⁷ was used. The DRT required the subject to retrieve, after an imposed 30-s delay, a hidden reward from one of the two receptacles

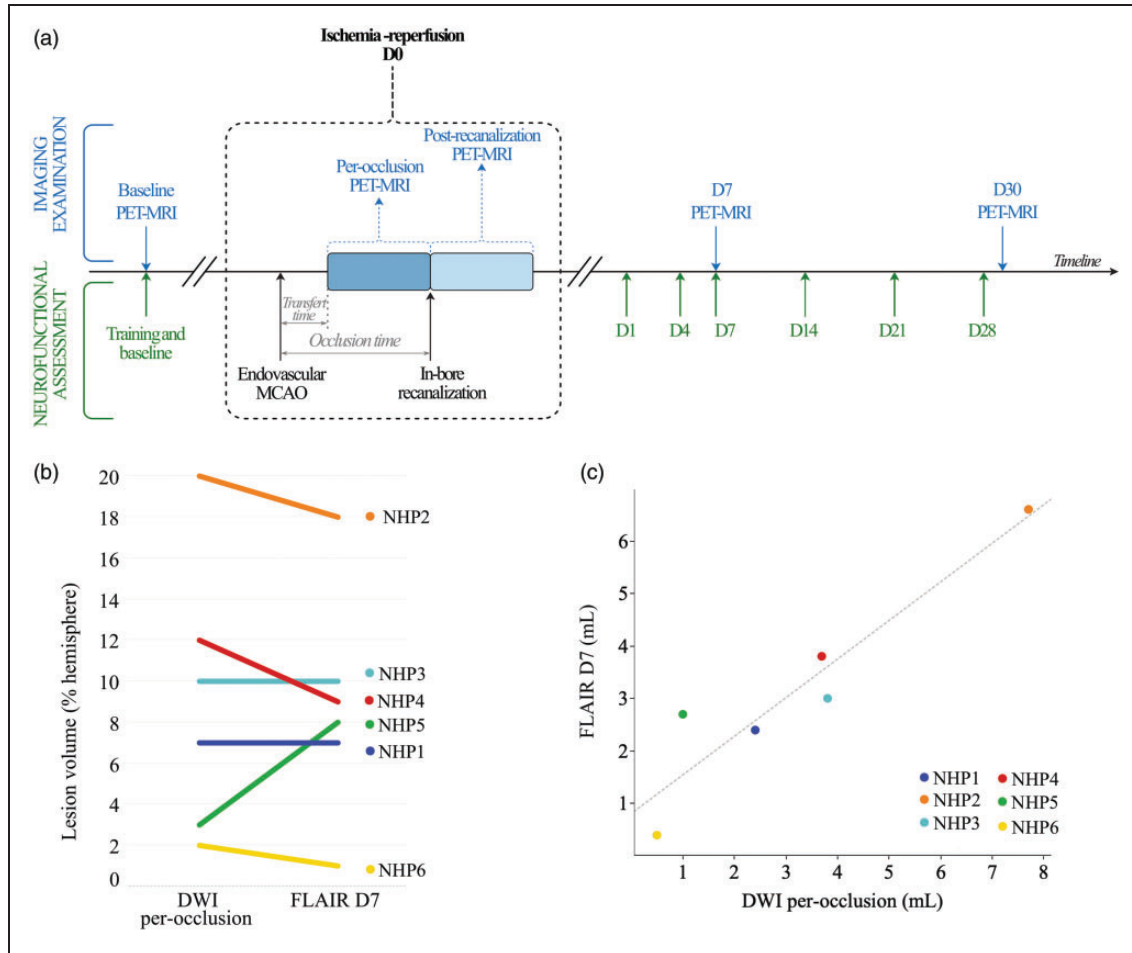


Figure 1. A reproducible endovascular MCAO procedure with per-occlusion and post-recanalization PET-MRI and positive thrombectomy-like outcome. We conducted the study in six animals that underwent temporary left MCAO, per-occlusion, post-recanalization, and day 7 and day 30 PET/MRI imaging (a). In parallel, we assessed neurofunctional status with a training and baseline assessment prior to any MCAO intervention, followed by a post-stroke evaluation at day 4, day 7, day 14, day 21 and day 28 (a). Individual progression (b) and linear regression (c) between lesion volume at occlusion (DWI+) and seven days later (FLAIR+) shows the relationship between the two parameters ($c - r = 0.886$, $p = 0.009$).

of the apparatus. The monkey was free to use either hand. Each monkey was trained on this task at least one month pre-surgery, and then longitudinally tested over the 28-day period post-stroke. Rewards were distributed randomly and equally between the left and right receptacles over the 10 trials of the task. Correct choice was used as an index of good cognitive performance. Further details are described in the Supplemental Materials and Methods.

Per-occlusion and post-revascularization image post-processing

Imaging data were wrapped on a common space using a *Macaca fascicularis* 3D template.¹⁸ Absolute PET-CBF parametric maps were computed after image-derived input function (IDIF) extraction in the aortic arch and

quantification using a one-tissue-compartment (Figure 1). PWI data were analyzed on Olea Sphere clinical software, v3.0 (Olea Medical, La Ciotat, France) to compute rCBF, Tmax and TTP maps.

Lesion expansion within the ischemic area was evaluated by standard DWI b1000, ADC maps, T2 FLAIR MRI and lesion volumes were segmented by an experienced neurologist (THC). A 79-label atlas covering all the brain was used to anatomically localize lesions.¹⁸

The influence of threshold on penumbra definition was investigated. In the PET-[¹⁵O]H₂O perfusion data, penumbra was defined as brain tissue with CBF < 0.2 ml/g/min, a standard clinical threshold for PET-MRI perfusion comparison^{19–22} that is also accepted for NHPs.²³ For MRI data, the parameter of choice and its threshold are far from consensual^{19,20,24,25}; therefore, using the most well-established parameters (Tmax and TTP),

MRI penumbra was defined after Tmax and TTP threshold values were evaluated by receiver operator characteristics (ROC) analysis against PET-[¹⁵O]H₂O CBF per-occlusion and D7 FLAIR volumes, similar to the clinical procedure for MRI and CT perfusion.^{24,26} Per-occlusion PET-[¹⁵O]H₂O was used as gold standard (with a threshold of CBF < 0.2 ml/g/min).

Collateral status, edema and blood–brain barrier (BBB) damage at reperfusion were evaluated. Collateral status during occlusion and the spatial extent and rapidity of vascular filling after revascularization were evaluated using a 5-point grading from DSC subtraction analysis to determine the filling phases (early, middle and late enhancement, respectively). The score was adapted to provide evaluation of more favorable profiles, equivalent to those of the American Society of Interventional and Therapeutic Neuroradiology/Society of Interventional Radiology.^{27,28} Blood–brain barrier (BBB) damage at reperfusion and late (day 7) hemorrhagic transformation was also evaluated from post-gadolinium FLAIR and T2* maps (Table S1).

To estimate post-revascularization damage progression, SST and AIT volumes were investigated^{29,30} after non-linear wrapping of hypoperfusion, DWI and FLAIR lesion masks on the common space. SST was defined as voxels either hypoperfused or in the DWI core lesion per-occlusion but outside the day-7 FLAIR lesion. AIT was defined as voxels neither hypoperfused nor in the DWI core lesion but inside the day-7 FLAIR lesion. These symptomatic salvaged and asymptomatic infarcted tissues were reported as absolute volumes and main location extent (number of anatomical regions, number of voxels per region, % of the voxel within the anatomic region).³¹

Statistical analysis

For functional assessments, statistical analyses used R software (v3.4.3). Non-parametric approaches were used to avoid the consequences of violation of normality. Spearman's rank correlation test was used to assess correlation between neurological score and infarct size. For both HDT and DRT tests, individual trials were averaged for each animal and each hand independently. Overall laterality was computed using a Friedman rank sum test across all days. Difference from baseline (Day 0 vs. Days 4–28) and laterality for each day individually was computed by Wilcoxon signed-rank tests. An alpha level of $p < 0.05$ was used to determine significance in all statistical tests; all tests were two-tailed.

For imaging parameters, statistical analyses used SPSS® v25.0 software (IBM Corp, Armonk, NY). Continuous variables were expressed as mean \pm standard deviation (SD), or median and interquartile range, according to their distribution. Continuous

variables were tested for differences with the Mann–Whitney U test. Spearman's rank test was used to assess correlation between per-occlusion DWI and D7 FLAIR. An alpha level of $p < 0.05$ was used to determine significance in all statistical tests.

Results

A translational and reproducible endovascular MCAO procedure compatible with per-occlusion and immediate post-recanalization PET-MRI and thrombectomy-like positive outcome

We conducted experimental procedures in six male cynomolgus macaques (*Macaca fascicularis*), aged 7.03 ± 0.11 years and weighing 9.69 ± 1.37 kg on occlusion day to evaluate the validity of the model using imaging and functional read-outs: per-occlusion core and penumbra, infarct size, and state-of-the-art behavioral evaluation (Supplemental Materials and Methods). We successfully achieved left MCAO (M2 segment) and in-bore revascularization without any procedural complications. All animals woke up without any major postoperative complications, and were evaluated serially as summarized in Figure 1(a). Tables S3 and S4 provide the monitoring and process parameters enabling a stable occlusion duration of between 96 and 134 min (median, 110.5 min). Successful recanalization was confirmed in all animals by TOF-MRA and resulted in favorable outcome, with 100% survival.

An expert neurologist performed segmentation of the DWI lesion (“DWI+”) and FLAIR lesion (“FLAIR+”) manually, since this is the only accepted method in clinical settings. Despite individual progression in ischemic lesion volume in each animal (Table 1), per-occlusion DWI lesion volumes were significantly higher than in post-recanalization ($p = 0.046$), suggesting either DWI reversal or an abrupt change in water distribution after the removal of the occluding material. Individual lesion volume progression between occlusion and seven days post-occlusion was more heterogeneous (Figure 1(b)), despite a clear relationship between the two lesion volumes (Figure 1(c); $r = 0.886$, $p < 0.01$). This serial analysis fits clinical data observed in the context of MT in humans, where the initial DWI lesion is a major factor in final lesion size.

Monkeys display significant motor and cognitive impairments that mimic those of stroke patients

In order to comply with the recommendations of the STAIR roundtable aimed at limiting failure of translation of therapeutic candidates from bench to bedside,^{32–35} we completed the characterization of our

Table 1. MRI per-occlusion DWI, post-revascularization DWI and day 7 FLAIR volumes and voxel-based shared volumes with day 7 FLAIR.

	Lesion volume mL (min-max)	Shared volume with FLAIR at D7	
		mL (min-max)	% (min-max)
DWI per-occlusion	3.0 (0.6–7.7)	1.0 (0.2–3)	45 (20–52)
DWI post-revascularization	1.7 (0–5) ^{a,b}	1.0 (0–2.2)	35 (0–40)
FLAIR D7	2.9 (0.4–6.6)	N/A	N/A

Note: All data are represented as median (range) of the six animals.

^aSignificantly different from per-occlusion DWI ($p < 0.05$).

^bSignificantly different from D7 FLAIR ($p < 0.05$).

stroke model by performing functional evaluations over the chronic post-stroke period.

In humans, the NIHSS is the reference scale for acute-phase stroke, as it predicts life expectancy, infarct size and residual disability. To achieve a closer approximation of the clinical paradigm, we designed a neurological scale fitting our model^{11,12,36}: the NHPNS. The monkeys were scored daily before and for one month after stroke induction (Figure 2(a)). Neurological deficits were observed 24 h after stroke induction, with impairment of consciousness, locomotion/coordination and sensitivity. Spearman's rank correlation test revealed a significant relationship between NHPNS score 24 h after MCAO and per-occlusion infarct size on DWI ($r = 0.93$, $p < 0.01$). Importantly, the relationship between NHPNS score at 24 h and final infarct size on FLAIR one week later was even stronger (Figure 2(b); $r = 0.98$, $p < 0.001$). Conversely, NHPNS score on day 7 did not correlate with infarct size measured the same day ($r = 0.54$, $p > 0.29$) and, on the following days, animals had NHPNS scores similar to baseline (Figure 2(a)). As in humans, these results indicate a strong correlation between NHPNS score specifically at the acute phase of stroke and final infarct size. To precisely characterize and quantify the neurological deficits in the chronic post-stroke period, the monkeys were thus subjected to fine and specific behavioral tests during the month following stroke induction.

Loss of voluntary movement control is the most common impairment after a stroke. Many individuals have unilateral motor dysfunctions in the upper and/or lower limbs, affecting their ability to perform activities of daily living. The initial deficit can improve, but in most cases upper-limb recovery is incomplete. We therefore performed a quantifiable and reproducible assessment of fine hand and digit movements on the HDT. Briefly, subjects had to collect rewards from receptacles of various diameters and locations with either hand, requiring increasing levels of fine motor control. Before stroke induction (Day 0), the monkeys performed the task successfully and quickly, retrieving all treats from the wells in less than 7 s (Figure 2(c)).

Importantly, there was no significant difference between the right and left limb performance (Figure 2(c), $p > 0.05$). In sharp contrast, four days after the vascular ictus, no animals were able to properly use the contralesional limb to retrieve the rewards (Figure 2(c); mean task latencies: Day 4, 18.6 s; Day 0, 6.3 s; Day 0 vs. Day 4: $p < 0.05$). This contralateral deficit with respect to baseline performance persisted throughout the test period, i.e. until post-stroke day 28 (Figure 2(c); Day 0 vs. Day 28: $p < 0.05$; Video S1). Moreover, contralesional limb performance was significantly poorer than ipsilesionally (Figure 2(c); Friedman rank sum test $p < 0.005$). With the ipsilateral arm, animals had some difficulty performing the task, but with a much less pronounced deficit than that of the contralateral arm, and with quick recovery (Figure 2(c); mean task latencies: Day 0, 5.7 s; Day 4, 9.9 s; Day 28, 5.5 s; Day 0 vs. Days 4–28: $p > 0.05$). Overall, the animals did not recover their contralateral fine motor skills during the month following stroke.

Most studies of stroke outcome have focused on physical sequelae, and few have examined cognitive aspects such as executive dysfunction, although these negatively affect the autonomy of stroke patients. Impaired executive function can manifest, for example, as deficits in memory, task flexibility and problem solving. To test the monkeys' cognitive functions, we used the DRT, a paradigm in which the monkey has to retrieve a hidden reward with either of their hands after an imposed delay. During the preoperative period (Day 0), the monkeys showed excellent cognitive ability in recovering the hidden treats on both sides (Figure 2(d); 100% correct choice). Stroke severely impaired cognitive performance on the contralateral side, with a significant decrease in percentage correct choice shortly after surgery (Figure 2(d); 20% and 57% correct responses on Day 4 and Day 7, respectively; $p < 0.05$ vs. Day 0). Moreover, the cognitive impairment tended to persist on the contralesional side over the long-term (Friedman rank sum test, $p < 0.005$). Interestingly, while three animals recovered completely by one month, various degrees of cognitive impairment

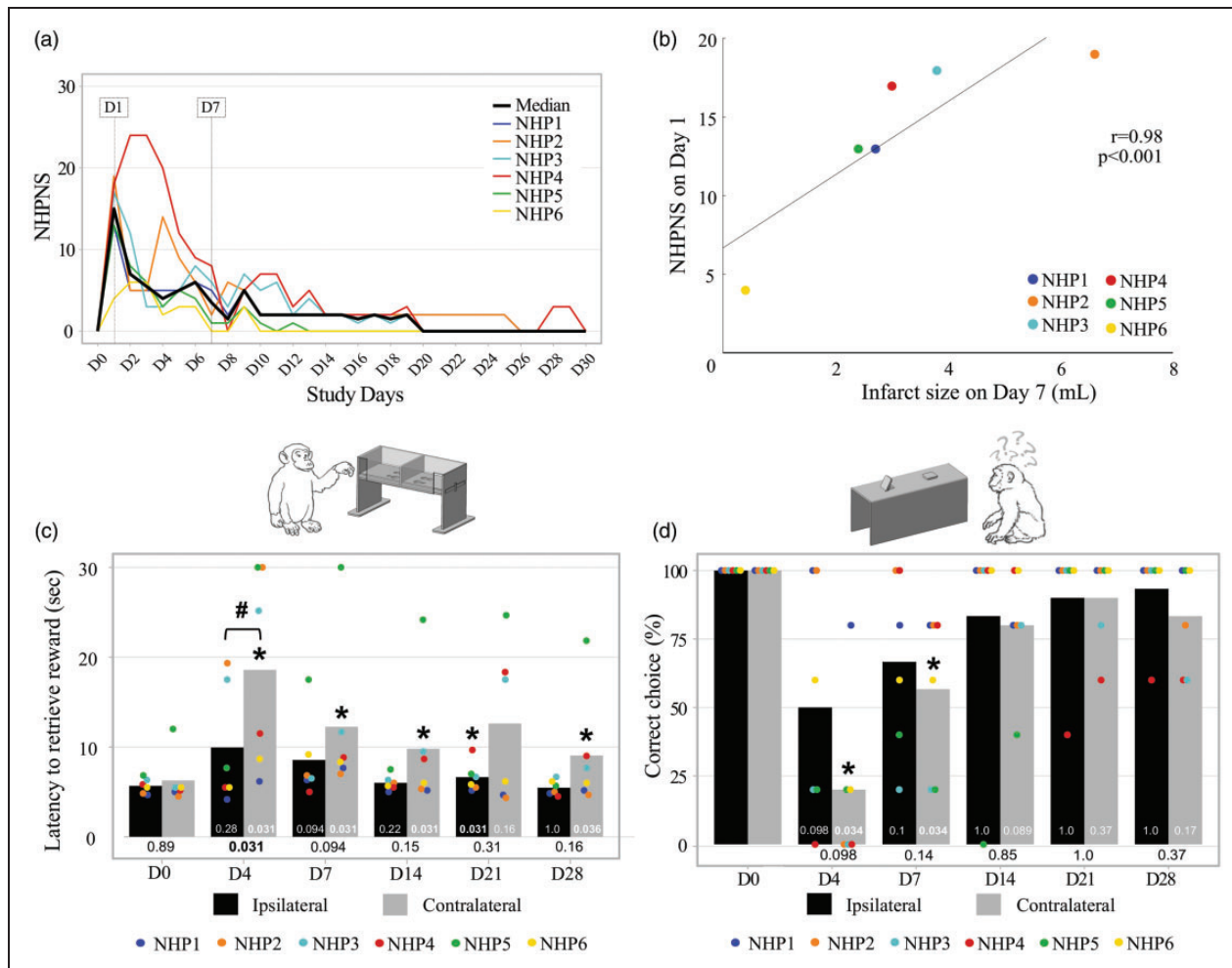


Figure 2. Monkeys had similar motor and cognitive impairments to those of human stroke patients. The Non-Human Primate Neurological Scale (NHPNS) reveals neurological deficits shortly after the cerebral injury (a), and is sensitive enough to predict the final infarct measured by FLAIR on Day 7 (b). The hand dexterity task (HDT) shows motor disruptions throughout the month following stroke induction. Mean reward retrieval latency is shown as a bar plot for each limb separately, and individual data are shown as colored dots (c). The delayed response task (DRT) highlights chronic impairment of cognitive skills after stroke induction. Mean percentage correct response is shown as a bar plot for each limb separately, and individual data are shown as colored dots (d). For c and d, difference day 0 vs. days 4, 7, 14, 21 or 28: * $p < 0.05$ (signed-rank test); Contralateral limb vs. Ipsilateral limb, # $p < 0.05$ (signed-rank test). P-values are specified for each condition.

persisted until Day 28 in the other three animals (Figure 2(d)). This indicates different patterns of cognitive recovery after MCAO, as observed clinically, with some animals showing persistent cognitive impairment even after one month.

Overall, these tests confirmed that the NHPNS is not fine enough to quantify neurological deficits in the long term. As outlined in a recent clinical study,³⁷ individual testing of fine motor and cognitive deficits is more relevant than a neurological score, and will be essential for further evaluation of neuroprotective interventions. The deficits revealed by our specific motor and cognitive tasks highlight this claim and the translational strength of our NHP model (Table S5).

Translational imaging read-outs similar to clinical MT trials

One major issue in both preclinical and clinical stroke is to evaluate ischemic and penumbra volumes by defining proper thresholds for segmentation.³⁸ As there are no MRI cutoff values in preclinical models, we performed PET- ^{15}O H₂O perfusion and PWI analysis in parallel. With PET, we used established methods to calculate quantitative cerebral blood flow (CBF, in mL/g/min) and generate parametric CBF maps. For MRI, time-to-peak (TTP, in s), T_{max} (in sec.) and relative CBF (rCBF, in mL/g/min) were calculated on robust clinical software with a manually defined

arterial input function (Supplemental method and Figure S1).²⁴ Hypoperfusion volumes were measured from the PET-CBF maps using the previously established NHP CBF threshold of <0.2 ml/g/min to define the ischemic region²³ (Figure 3, step 3). Less stringent PET thresholds were also tested, as previously reported²³ (Table 2). We finally validated $TTP >1$ s and $Tmax >2$ s as optimal MRI thresholds in this model (Supplemental methods and Figure S2).

The areas of per-occlusion perfusion defects assessed with both techniques (PET and either PWI-TTP or Tmax) were colocalized in 68% and 69% of cases for Tmax and TTP, respectively, and the PWI volumes

were significantly larger than those obtained with PET perfusion imaging ($p=0.028$ and $p=0.043$, respectively; Table 2). As collaterals are major actors during ischemia, we also graded the degree of collaterality, by dedicated post-processing of MRI PWI (Supplemental Figure S1, last step and Table S6).²⁷ High collaterality grade in this model is therefore a possible explanation for the larger ischemic volumes obtained on MRI than on PET, where a stricter ischemia threshold was used (Table 2).

To further estimate ischemia and reperfusion imaging metrics, we developed a dedicated post-processing PET-MRI workflow for voxel-based analysis (Figure 3).

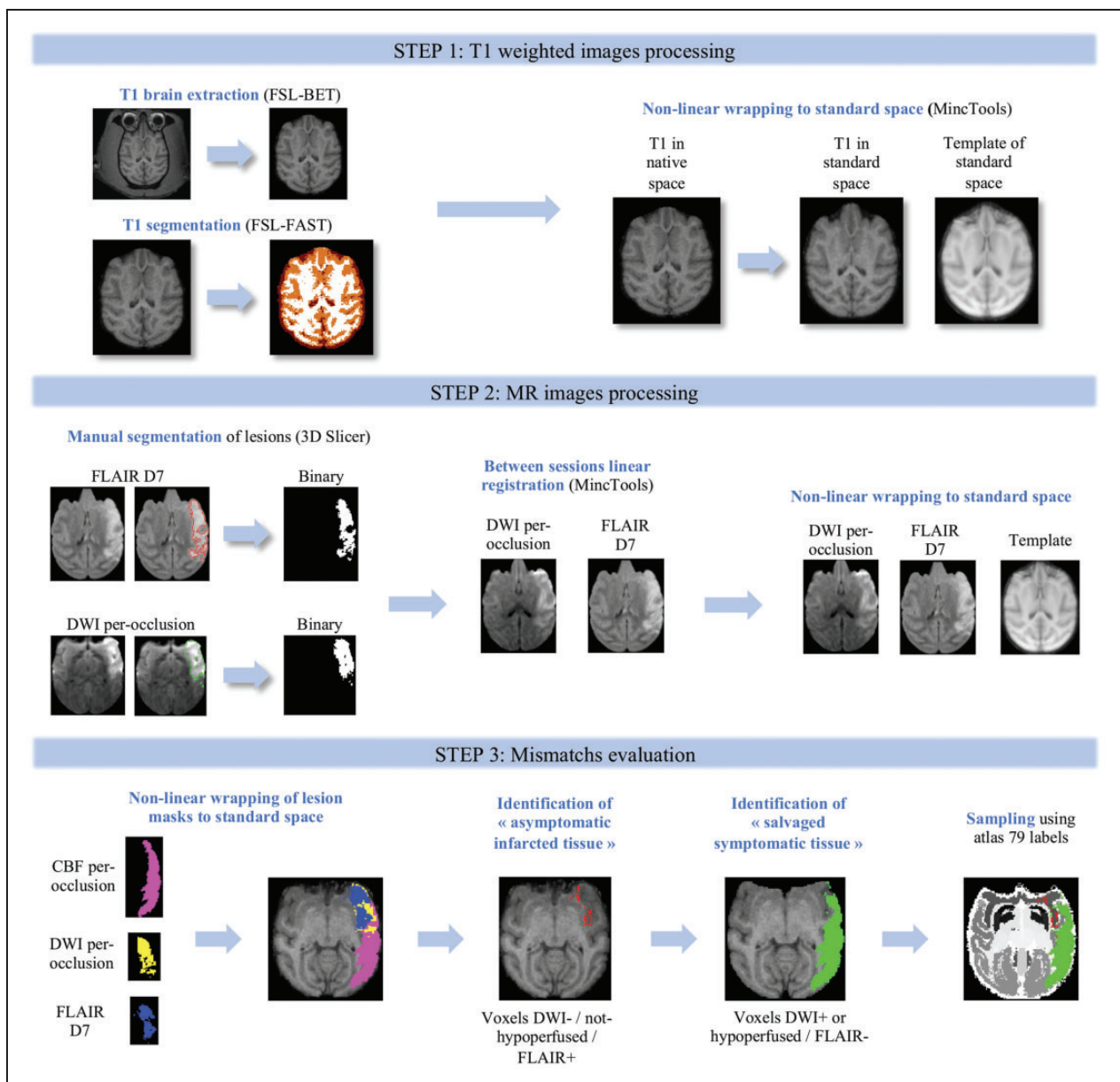


Figure 3. Translational imaging read-outs similar to clinical MT trials. We set up innovative, rigorous and reproducible imaging data post-processing, divided in three steps, to obtain full lesion characterization.

Table 2. PET and MRI perfusion volumes over time and voxel-based shared volumes.

	Perfusion defect per-occlusion		Penumbra (Perfusion-DWI)		Shared volume with PET per-occlusion (PET CBF < 0.2 mL/g/min)		Reperused volume		Shared volume with PET post-revascularization (PET CBF < 0.2 mL/g/min)		Shared per-occlusion with FLAIR lesion at D7		Shared post-revascularization defect with FLAIR lesion at D7	
	mL (min-max)	% (min-max)	mL (min-max)	% (min-max)	mL (min-max)	% (min-max)	mL (min-max)	% (min-max)	mL (min-max)	% (min-max)	mL (min-max)	% (min-max)	mL (min-max)	% (min-max)
PET CBF < 0.2 mL/g/min	2.2 (0.7-13)	1.6 (0.3-11.8)	NA	NA	0.6 (0-8.6)	67 (0-100)	NA	NA	0.4 (0.1-3.2)	29 (2-51)	0 (0-3.1)	0 (0-47)		
PET CBF < 0.24 mL/g/min	3.6 (3.4-15.8) ^{**†}	3.4 (2.3-14.3)	NA	NA	1.3 (0-12.3)	62 (11.5-100)	NA	NA	0.8 (0.2-3.8)	39 (8-70)	0.3 (0-3.6)	9 (0-54)		
PET CBF < 0.27 mL/g/min	7.5 (5-19.3) ^{abc}	6.5 (3.4-17.7)	NA	NA	5.7 (0-15)	33.7 (0-100)	NA	NA	1.2 (0.2-3.9)	46 (20-83)	0.8 (0-3.7)	25 (0-58)		
T _{max} > 2 s	13.5 (9.3-16.3) ^{abc}	12.2 (4.7-14.4)	1.1 (0.6-6.9)	68 (30-100)	5.9 (0-15)	63 (0-100)	0.3 (0-5)	4 (0-70)	1.9 (0.3-3.2)	72 (47-83)	0.5 (0-2)	16 (0-83)		
TTP > 1 s	10.6 (6.9-14.6) ^{abc}	9.6 (5.6-14.2)	0.7 (0.5-5.7)	69 (22-100)	3.9 (0-12.3)	66 (0-100)	0 (0-0.8)	0 (0-70)	1.4 (0.3-3.5)	53 (34-77)	0.1 (0-1.9)	4 (0-50)		

Note: All data are represented as median (range) of the six animals.

^aSignificantly different from FLAIR D7 lesion volume ($p < 0.05$).

^bSignificantly different from DWI per-occlusion lesion volume ($p < 0.05$).

^cSignificantly different from PET-CBF per-occlusion lesion volume (PET-CBF < 0.2 mL/g/min; $p < 0.05$).

Even with the strict PET threshold of 0.2 mL/min/g, the penumbra, defined as non-DWI+ per-occlusion hypo-perfused voxels, was present in all cases, and ranged from 0.3 to 11.8 mL (Table 2), consistent with clinical eligibility criteria for MT.

We then considered more advanced imaging parameters related to outcome after recanalization. Among these, no-reflow was present in 50% of cases with the PET CBF threshold, reproducing recent clinical findings of no or low reperfusion despite successful recanalization, a target for adjunct therapy after MT.³⁹ Of note, perfusion was back to normal with both PET and MRI by day 7.

Voxel-based analysis enables follow-up of lesion location over time and reveals that lesion progression is frequent and associated with complex neuro-functional outcome

The reproducibility of the infarct core locations and the variability of their size were shown by lesion overlays in all animals (Figure 4(a)). Per-occlusion DWI lesions involved both superficial territories (frontal, temporal and parietal cortex) and deep structures (limbic system and basal ganglia), consistent with clinical findings⁴⁰ (Figure 4(b)). Localization patterns for per-occlusion PET ischemia, post-recanalization DWI+ and day-7 FLAIR+ ischemic lesions were close, but with region-specific changes (Figure 4(a) to (e), with individual cases in Figure S3 and in 3D in Movie S2).

Lesion volumes on per-occlusion DWI and day-7 FLAIR were globally comparable ($p = 0.753$), but with maximum shared volumes of only 52% (Table 1). To better understand this change in lesion location and extension in specific brain regions between the various time points, voxel-based analysis was performed, similar to previous clinical studies⁴¹ (Figure 3, last step). Interestingly, two distinct patterns of progression were seen in all cases, reflecting the complex post-recanalization behavior of brain tissue (Figure 5 (a) and Figure S4 for individual cases): (a) “symptomatic salvaged tissue” (SST), corresponding to initially damaged but finally salvaged tissue (i.e. voxels positive on per-occlusion DWI or hypoperfused on per-occlusion PET perfusion, but negative on FLAIR at day 7); and (b) “asymptomatic infarcted tissue” (AIT) corresponding to initially normal but finally infarcted tissue (i.e. voxels negative on per-occlusion DWI and normally perfused on per-occlusion PET perfusion, but positive on FLAIR at day 7), representing 45% of the final infarct size (Figure 5(b)).

SST was mainly localized in the ventral frontal cortex, inferior parietal cortex, superior temporal

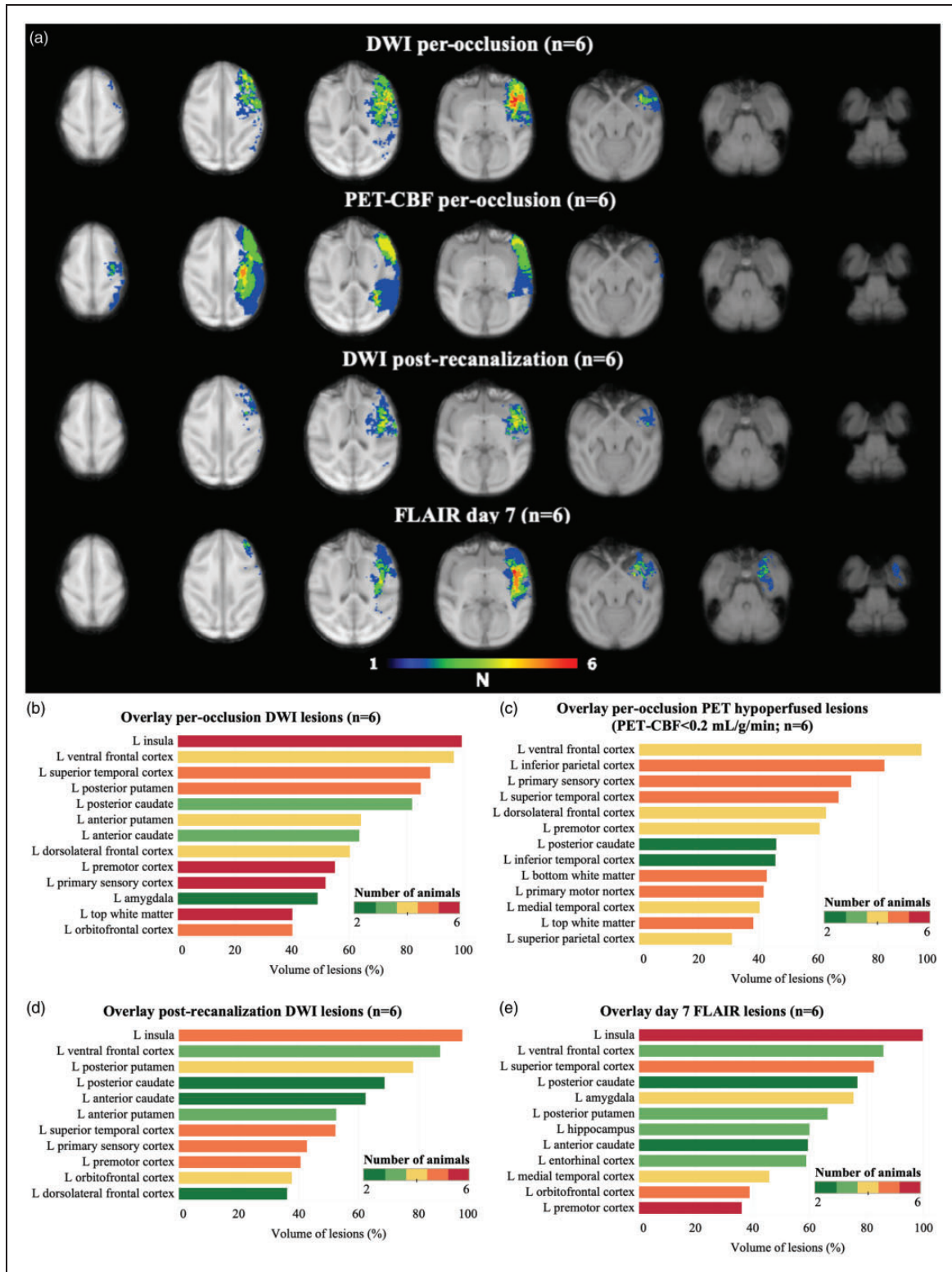


Figure 4. Voxel-based analysis enables follow-up of lesion location over time. Lesion overlap ($n = 6$ animals) after registration on the atlas showed shared lesion locations on per-occlusion DWI (upper row), per-occlusion PET-CBF lesions (second row), post-recanalization DWI (third row) and day 7 MRI FLAIR (lower row). The color bar indicates the number of overlapping lesions (a). Voxel-based analysis of lesion location in each atlas region (with lesion volume $>30\%$ of region) is displayed in bar graphs for per-occlusion DWI lesion overlap (b), per-occlusion PET-hypoperfused lesion overlap (c), post-recanalization DWI lesion overlap (d) and day 7 FLAIR lesion overlay (e). Colors indicate the number of animals with lesions in the corresponding atlas region.

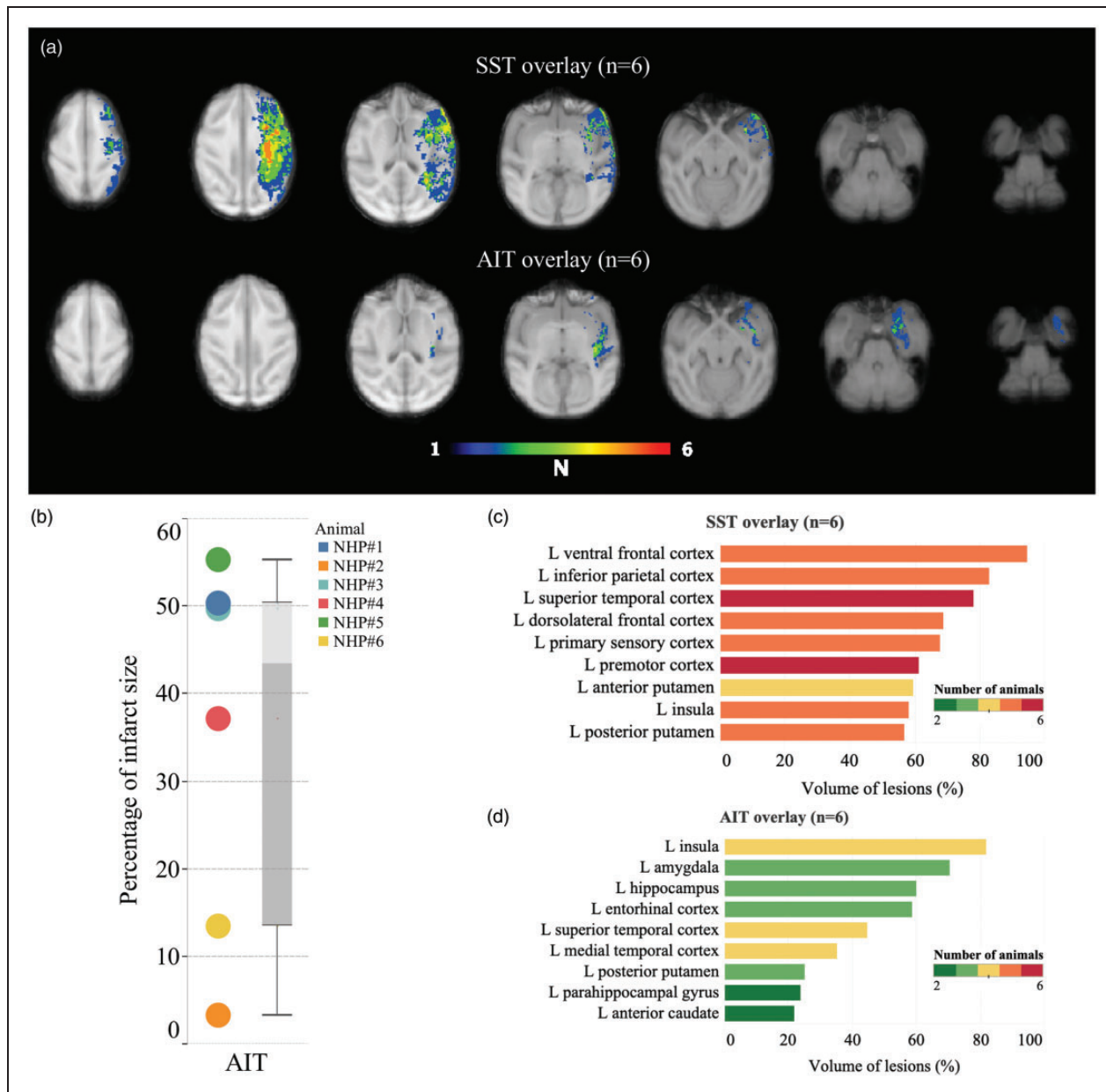


Figure 5. Voxel-based analysis shows that lesion progression is frequent and associated with complex neuro-functional outcome. Lesion overlap plots of salvaged symptomatic tissue (SST; upper row) and asymptomatic infarcted tissue (AIT; lower row) from all animals ($n = 6$) (a). The color bar indicates the number of overlapping lesions. Post-recanalization progression (AIT) volume contributes significantly to final infarct size: AIT (voxels negative on per-occlusion DWI and normally perfused on per-occlusion PET perfusion, but positive on FLAIR at day 7), expressed as percentage of final infarct size, represent 45% of final infarct size (left, individual values as dots; right, box-plots) (b). Bar graphs representing the percentage of SST (c) and AIT (d) lesions in each atlas region ($n = 6$). Colors indicate the number of animals with lesions in the corresponding atlas region. SST was mainly localized in the ventral frontal cortex, inferior parietal cortex, superior temporal cortex, dorsolateral frontal cortex, primary sensory cortex, and AIT in the superior temporal cortex, medial temporal cortex, insula, hippocampus and amygdala.

cortex, dorsolateral frontal cortex and primary sensory cortex, and AIT in the superior temporal cortex, medial temporal cortex, insula, hippocampus and amygdala (Figure 5(c) and (d)). No foci of AIT outside the territory of the occluded artery were observed, suggesting a good specificity of our model.

Discussion

This translational NHP ischemic stroke model with a transient MCAO was induced by a minimally invasive endovascular approach, with 100% postoperative survival. The consequences of MCAO were characterized

by per-occlusion and longitudinal state-of-the-art imaging, in parallel with fine neurofunctional assessment and voxel-based imaging analysis. This new ischemic stroke model in the reference NHP species for preclinical trials (*Macaca fascicularis*) is the first to assess the role of ischemia–reperfusion damage in final infarct size by showing, locating and measuring ischemic regression and progression. It was associated with persistent deficits in animals' motor and cognitive functions. The model closely mimics progression in human stroke after recanalization and is thus ideal to assess the efficacy of novel per-ischemia and post-recanalization neuroprotection interventions to be used in conjunction with MT.

A novel ischemic stroke model with complete characterization

The ideal ischemic stroke model should be minimally invasive, in order to minimize postoperative impairment, pain and stress.^{1–3,42} Above all, occlusion should be reversible and compatible with per-occlusion and per-recanalization imaging, so as to mimic an MT setting. Besides, the ideal ischemic stroke model should also provide significant cerebral penumbra, in order to reproduce the clinical MT issues as closely as possible. Compared to surgical approaches, endovascular methods for ISMs in NHPs are minimally invasive and easier to perform. They significantly reduce traumatic pain (compared to craniotomy or transorbital approaches) and allow survival and fast recovery, enabling longitudinal behavioral assessment.⁹ Intraarterial thrombus administration would have made the model even more realistic. However, as highlighted in the review from Herrmann et al.,⁴³ some limitations exist as the unpredictable final destination of the clot and its difficulty to be retrieved (see Supplemental Discussion). Our model successfully induced reproducible cortical-subcortical infarction in the MCA territory with (i) the possibility of assessing the infarct core and cerebral penumbra by PET-MRI, (ii) imaging of ischemia–reperfusion-related damage and (iii) evaluation of motor and cognitive deficits by a complete neurofunctional assessment. On this endovascular approach with deployment of a coil in the MCA M2 segment, all animals recovered from the operation without any complications (e.g. vessel perforation, unintended embolic stroke, intracranial hemorrhage, vessel dissection or groin complications) and could be monitored by imaging, clinical and functional assessment for one month.

We compared our model to those previously published, using transient and reversible ischemic stroke models based on endovascular approaches (excluding those using surgical approaches, given their complexity

and invasiveness). Previous studies on stroke models based on endovascular approaches reported mortality between 8.7% and 83.3% (Supplemental Table S5). Our model achieved ischemic stroke detectable by imaging with neurological deficits in all animals. In comparison, in the literature, these rates range from 33.3% to 100% (Supplemental Table S5).

As expected, the infarct core volumes obtained with our ischemic stroke model were globally small and in good agreement with volumes obtained with the models based on M2 occlusion.^{3,6} In these models, infarct core volumes showed lower inter-individual variability than with more proximal (M1) occlusion.^{3,8,44} With a hemisphere volume of 35 mL in the cynomolgus macaque, the range of the infarct core volumes seven days after revascularization combined with the cerebral penumbra volumes was close to that observed in human stroke relative to the respective hemisphere volumes.⁴⁵ As in clinic, many factors may contribute to these variations such as degree of pial collaterality⁴⁶ and the potential presence of slow versus fast progressors among the animals as recently reported in a dog model⁴⁷ (see Supplemental Discussion). This highlights the reliability of the model to induce ischemia and perfusion impairment similar to the hallmark pathophysiological processes of natural stroke.

Clinically relevant imaging methods applied to NHP

Accurate detection of both hypoperfusion and penumbra is crucial in AIS. Many investigations on both PET and MRI measurements of perfusion have been made to optimize the hypoperfusion detection threshold. Based on human PET-perfusion studies, a CBF threshold of <20 mL/100 g/min is well-established.^{19,20} Most studies comparing this PET threshold with classical human PWI parameter thresholds (e.g. Tmax >6 s) were conducted on different scanners (MRI, then PET) or different days (MRI per-occlusion vs. MRI FLAIR at days 2–7).^{19,20} These thresholds were established in non-reperfused infarction, where the hypoperfused area was assumed to correspond to the final lesion. In the MT era, there is a controversy about the performance of these thresholds, opening a window for multiple methodological studies to optimize perfusion assessment.^{19,20,24} Hybrid PET-MRI scanners are now able to assess perfusion simultaneously on PET and MRI. So far, only one paper compared PET and MRI perfusion with simultaneous measurements in both pre-clinical and clinical stroke.⁴⁸ Similar to our findings, Tmax and TTP threshold values in a sheep stroke model with permanent occlusion were also different from clinical ones, with a better definition of the penumbra with the combined PET perfusion and MRI diffusion.⁴⁸ To date,

MRI perfusion parameters have not been validated in NHPs, which led us to develop a methodology to predict the tissue at risk of infarction with PWI (Figure S2). ROC analysis and volume comparisons showed significantly different thresholds than in human studies, which could be explained by NHP physiology and naturally developed collateral circulation. Although the present number of animals was too small to fully establish the performance of the tested PWI parameters (i.e. Tmax and TTP), the threshold values that we defined and the resulting hypoperfusion and penumbra volumes were consistent with the PET data, especially when using less strict PET thresholds (Table 2 and Supplemental Figure S2). Further studies are needed to fully validate dedicated PWI parameters for NHP ischemia–reperfusion studies.

Clinically relevant functional deficits in the endovascular NHP model

Of the parameters taken into consideration for the evaluation of novel treatments in experimental stroke models, functional outcome is one of the most important. Whereas neurofunctional tests in rodent stroke models are subject to high variability and are often difficult to interpret, neurological deficits and functional recovery in NHPs can be assessed both qualitatively and quantitatively, as we did by means of three non-aversive behavioral tests: NHPNS, HDT and DRT. In the acute phase of stroke, NHPNS showed classical deficits consistent with cerebral ischemia (e.g. drowsiness, impairment of motor and somesthetic systems) and was strongly predictive of final cerebral infarct size. As in humans, functional recovery was more or less rapid, a fact directly related to the size and location of the lesion like the NIHSS score does in humans.⁴⁹ These results show that such a neurological scale, which is easy and rapid to implement, can evaluate short-term, but not long-term, functional deficits. The complementary fine behavioral analyses demonstrated specific chronic deficits underlying the stroke, with no evidence of significant recovery over time.

HDT specifically assesses motor functions, disregarding compensatory behaviors that could bias the results of observational functional tests: whereas NHPNS score went back to baseline after 10 days, most animals still showed deficits on HDT at one month. The disabilities of monkeys' digits and hand were contralateral, a result consistent with the left (ipsilateral) cerebral lesions. In addition, the motor dysfunctions identified in our NHP model were close to those observed in stroke patients: while partial recovery of motor activity often occurs spontaneously, about half of patients show chronic disabilities that impact on autonomy and social activities.⁵⁰ Our

animals displayed the same ratio of disability, which underscores the translational aspect of our model.

The cognitive profile assessed on DRT was also negatively affected after stroke induction in monkeys. While visuospatial neglect, aphasia, or apraxia are well-identified consequences of stroke, other cognitive impairments such as in executive functions were less often investigated, despite being severely disabling. The DRT assesses executive functions as a product of the coordinated operation of various processes (data capture, selection of relevant information, memorization of a mental representation, programming of a response, validation of the response confirming the rule used, prediction of the future response) to accomplish a particular goal in a flexible manner.¹⁵ The cognitive deficit observed on the contralesional side was coherent with the literature on NHP.⁵¹ Indeed, while contralateral spatial neglect occurs mainly after lesions in the right hemisphere in human patients, contralateral neglect-like behavior was present in some monkeys with left MCAO, confirming the lack of clearly defined laterality in NHPs. Interestingly, the residual dysexecutive behavior seen in the present study was consistent with the damage to cortical regions per se, but also with the chronic underlying disturbance of frontal-subcortical and medial temporal limbic circuits. Once again, these preclinical data are in line with clinical observations, and strengthen the relevance of the model.

Voxel-based analysis showed ischemia–reperfusion damage in specific areas

We also documented the presence of infarcted tissue that was firstly assumed not to be part of the final infarct (i.e. “non-core-non-penumbra” tissue – Figure 5). This phenomenon was found in all animals and, more substantially, in four animals that had more than 1.2 mL of asymptomatic infarcted tissue (AIT), with a median volume of 1.3 mL (45% relative to median final infarct and 3.7% relative to hemisphere volume). Similar observations linked with clinical course were reported a few years ago²⁹ and need to be confirmed in clinical cohorts with final infarct size measured on FLAIR MRI within a similar time frame after thrombectomy. The progressing zones in the present study corresponded to regions known to be highly vulnerable to transient ischemia in patients.⁵²

One limitation of our study was the small number of animals. It precluded reaching statistical significance to establish a link between lesion location, asymptomatic infarcted tissue and clinical outcome. Also, a major difference compared to patients was the absence of co-morbidities and their potential impact on ischemia–reperfusion injury. From this initial experience, we propose that the imaging metrics of AIT and SST

should be further evaluated as imaging biomarkers of therapeutic effectiveness in both pre-clinical and clinical thrombectomy studies.^{53–54}

Conclusion

We set up a robust translational thrombectomy-like model of stroke, with extensive characterization of lesions during occlusion and after recanalization. Combined per-occlusion and immediate post-recanalization PET-MRI imaging enabled validation of perfusion MRI thresholds to assess the ischemic penumbra, the target of neuroprotection intervention. The reproducible and fully accessible PET-MRI imaging protocol was enriched by complete neurofunctional evaluation. The NHPNS assesses the general status of subjects early after cerebral injury, and is sensitive enough to predict the final infarct size. The HDT and the DRT reveal, with high specificity, motor disruption and dysexecutive behavior related to cortical-subcortical damage. Taken together, these complementary tasks are highly sensitive functional tools for the studies of regeneration and repair after stroke. In addition, based on an original voxel-based analysis, we also defined quantitative imaging metrics (i.e. AIT and SST) that should enable evaluation of future per-ischemia and post-recanalization neuroprotective drugs or strategies. We think that reproducible science and groundbreaking advances can only be made by sharing data and methodology, so anyone interested could reproduce, confirm and enhance this study with new results and preclinical neuroprotection trials.

Funding

The author(s) disclosed receipt of the following financial support for the research, authorship, and/or publication of this article: This work was supported by the ANR CYCLOPS (ANR-15-CE17-0020) and the RHU MARVELOUS (ANR-16-RHUS-0009) of Université de Lyon, within the program Investissements d'Avenir operated by the French National Research Agency (ANR). The PhD salaries of Oceane Wateau (Cifre, Cynbiose) and Justine Debatisse (Cifre, Siemens) are co-funded by the French Ministry of Higher Education and Research (ANRT).

Acknowledgments

We acknowledge AC. Lukaszewicz for her contribution in the anesthesia procedure, G. Boudou for his help in performing neurofunctional tests, M. Wiart and M. Paillard for fruitful discussions on stroke models and ischemia-reperfusion injury.

Declaration of conflicting interests

The author(s) declared no potential conflicts of interest with respect to the research, authorship, and/or publication of this article.

Authors' contributions

Emmanuelle Canet-Soulas conceived and designed the study; Omer F. Eker, Mohamed Aggour designed the endovascular procedure; Tae-Hee Cho, Emmanuelle Canet-Soulas, Nicolas Costes, Marjorie Villien, Thomas Troalen designed the imaging protocol; Océane Wateau, Michaël Verset, Hugues Contamin, Tae-Hee Cho, Véronique Agin, Denis Vivien designed the clinical neuroscore and neurofunctional tests; Michaël Verset, Océane Wateau, Karine Portier, Adrien Oudotte designed the anesthesia and monitoring procedure; Justine Debatisse, Tae-Hee Cho, Nikos Makris, Nicolas Costes, Emmanuelle Canet-Soulas designed the imaging post-processing pipeline.

Omer F. Eker, Mohamed Aggour performed the endovascular procedure; Justine Debatisse, Nicolas Costes, Inés Mérida, Marjorie Villien, Nikos Makris, Tae-Hee Cho and Emmanuelle Canet-Soulas performed imaging acquisition and imaging agent administration; Didier Le Bars, Sophie Lancelot and Christian Tourvieille performed radiopharmaceutical synthesis; Océane Wateau, Fabrice Taborik, Michaël Verset, Karine Portier, Adrien Oudotte, Jean-Baptiste Langlois, Christelle Léon performed study management, anesthesia and monitoring.

Justine Debatisse, Tae-Hee Cho, Omer F. Eker, Emmanuelle Canet-Soulas analyzed the imaging data; Océane Wateau, Joachim Confais, Véronique Agin, Denis Vivien analyzed the neurofunctional data.

Omer F. Eker, Justine Debatisse, Océane Wateau, Joachim Confais, Véronique Agin, Tae-Hee Cho, Emmanuelle Canet-Soulas interpreted the data.

Omer F. Eker, Justine Debatisse, Océane Wateau, Joachim Confais, Véronique Agin, Emmanuelle Canet-Soulas drafted the manuscript.

Norbert Nighoghossian, Denis Vivien, Tae-Hee Cho, Michel Ovize, Omer F. Eker, Véronique Agin, Emmanuelle Canet-Soulas revised the manuscript critically for important intellectual content.

All authors approved the final version of the manuscript submitted.

Data and materials availability

All data generated or analyzed during this study are included in this published article and its supplementary Materials.

Ethics approval

All experiments were carried out in accordance with the European Directive 2010/63/UE and ARRIVE guidelines (Animal Research: Reporting in Vivo Experiments) and were approved by the Animal Welfare Body of Cynbiose and the Ethics Committee of VetAgro-Sup (C2EA-18) and CELYNE (C2EA-42) and authorized by the Ministry of Higher Education, Research and Innovation under numbers

APAFIS#4702 and 8901. The animal facility of Cynbiose is fully accredited by the Association for Assessment and Accreditation of Laboratory Animal Care (AAALAC).

Comment

Endovascular mechanical thrombectomy is dramatically changing the management of acute ischemic stroke. New pre-clinical models are needed to evaluate ischemia–reperfusion damage in the era of this major medical advance, with both longitudinal imaging and neurofunctional read-outs for future per- and post-ischemia neuroprotection trials. In the present work, we developed a reversible, survivable endovascular method of inducing ischemia–reperfusion stroke in non-human primate models with imaging and behavioral read-outs, as close as possible to clinical observations. It is the pre-requisite validation study and is part of a larger pre-clinical study which complied to the ARRIVE guidelines.

References

1. Fukuda S, del Zoppo GJ. Models of focal cerebral ischemia in the nonhuman primate. *ILAR J* 2003; 44: 96–104.
2. Cook DJ, Teves L, Tymianski M. A translational paradigm for the preclinical evaluation of the stroke neuroprotectant Tat-NR2B9c in gyrencephalic nonhuman primates. *Sci Transl Med* 2012; 4: 1–9.
3. Zhao B, Shang G, Chen J, et al. A more consistent intraluminal rhesus monkey model of ischemic stroke. *Neural Regen Res* 2014; 9: 2087.
4. Freret T, Bouet V, Toutain J, et al. Intraluminal thread model of focal stroke in the non-human primate. *J Cereb Blood Flow Metab* 2008; 28: 786–796.
5. Rodriguez-Mercado R, Ford GD, Xu Z, et al. Acute neuronal injury and blood genomic profiles in a nonhuman primate model for ischemic stroke. *Comp Med* 2012; 62: 427–438.
6. De Crespigny AJ, D'Arceuil HE, Maynard KI, et al. Acute studies of a new primate model of reversible middle cerebral artery occlusion. *J Stroke Cerebrovasc Dis* 2005; 14: 80–87.
7. Gauberti M, Obiang P, Guedin P, et al. Thrombotic stroke in the anesthetized monkey (*Macaca mulatta*): characterization by MRI—a pilot study. *Cerebrovasc Dis* 2012; 33: 329–339.
8. Wu D, Chen J, Wang B, et al. Endovascular ischemic stroke models of adult rhesus monkeys: a comparison of two endovascular methods. *Sci Rep* 2016; 6: 1–10.
9. Fan J, Li Y, Fu X, et al. Nonhuman primate models of focal cerebral ischemia. *Neural Regen Res* 2017; 12: 321–328.
10. Shi H, Liu KJ. Cerebral tissue oxygenation and oxidative brain injury during ischemia and reperfusion. *Front Biosci* 2007; 12: 1318–1328.
11. Spetzler RF, Selman WR, Weinstein P, et al. Chronic reversible cerebral ischemia: evaluation of a new baboon model. *Neurosurgery* 1980; 7: 257–261.
12. Mack WJ, King RG, Hoh DJ, et al. An improved functional neurological examination for use in nonhuman primate studies of focal reperfusion cerebral ischemia. *Neurol Res* 2003; 25: 280–284.
13. Moore TL, Killiany RJ, Pessina MA, et al. Assessment of motor function of the hand in aged rhesus monkeys. *Somatosens Mot Res* 2010; 27: 121–130.
14. Moore TL, Killiany RJ, Pessina MA, et al. Recovery from ischemia in the middle-aged brain: a nonhuman primate model. *Neurobiol Aging* 2012; 33: 619.e9–619.e24.
15. Darusman HS, Call J, Sajuthi D, et al. Delayed response task performance as a function of age in cynomolgus monkeys (*Macaca fascicularis*). *Primates* 2014; 55: 259–267.
16. Wang M, Yang Y, Wang CJ, et al. NMDA receptors subserve persistent neuronal firing during working memory in dorsolateral prefrontal cortex. *Neuron* 2013; 77: 736–749.
17. Davachi L, Goldman-Rakic PS. Primate rhinal cortex participates in both visual recognition and working memory tasks: functional mapping with 2-DG. *J Neurophysiol* 2001; 85: 2590–2601.
18. Ballanger B, Tremblay L, Sgambato-Faure V, et al. A multi-atlas based method for automated anatomical *Macaca fascicularis* brain MRI segmentation and PET kinetic extraction. *Neuroimage* 2013; 77: 26–43.
19. Zaro-Weber O, Moeller-Hartmann W, Siegmund D, et al. MRI-based mismatch detection in acute ischemic stroke: optimal PWI maps and thresholds validated with PET. *J Cereb Blood Flow Metab* 2017; 37: 3176–3183.
20. Reimer J, Montag C, Schuster A, et al. Is perfusion MRI without deconvolution reliable for mismatch detection in acute stroke? Validation with 15 O-positron emission tomography. *Cerebrovasc Dis* 2018; 46: 16–23.
21. Muir KW, Buchan A, von Kummer R, et al. Imaging of acute stroke. *Lancet Neurol* 2006; 5: 755–768.
22. Takasawa M, Jones PS, Guadagno JV, et al. How reliable is perfusion MR in acute stroke? Validation and determination of the penumbra threshold against quantitative PET. *Stroke* 2008; 39: 870–877.
23. Baron J-C, Moustafa RR. Perfusion thresholds in cerebral ischemia. In: Geoffrey AD, Jean-Claude B, Stephen MD, et al. (eds) *The ischemic penumbra* 21: 32, 2007, pp. 21–35.
24. Nasel C, Klickovic U, Kührer HM, et al. A quantitative comparison of clinically employed parameters in the assessment of acute cerebral ischemia using dynamic susceptibility contrast magnetic resonance imaging. *Front Physiol* 2019; 10: 1–13.
25. Wouters A, Christensen S, Straka M, et al. A comparison of relative time to peak and tmax for mismatch-based patient selection. *Front Neurol* 2017; 8: 1–7.
26. Lin L, Cheng X, Bivard A, et al. Quantifying reperfusion of the ischemic region on whole-brain computed

- tomography perfusion. *J Cereb Blood Flow Metab* 2017; 37: 2125–2136.
27. Makris N, Chamard L, Mikkelsen IK, et al. Acute reperfusion without recanalization: serial assessment of collaterals within 6 h of using perfusion-weighted magnetic resonance imaging. *J Cereb Blood Flow Metab* 2019; 39: 251–259.
 28. Higashida RT, Furlan AJ. Trial design and reporting standards for intra-arterial cerebral thrombolysis for acute ischemic stroke. *Stroke* 2003; 34: 2774.
 29. Alawneh JA, Jones PS, Mikkelsen IK, et al. Infarction of ‘non-core-non-penumbra’ tissue after stroke: multivariate modelling of clinical impact. *Brain* 2011; 134: 1765–1776.
 30. Harston GWJ, Carone D, Sheerin F, et al. Quantifying infarct growth and secondary injury volumes: comparing multimodal image registration measures. *Stroke* 2018; 49: 1647–1655.
 31. Cheng B, Forkert ND, Zavaglia M, et al. Influence of stroke infarct location on functional outcome measured by the modified Rankin scale. *Stroke* 2014; 45: 1695–1702.
 32. Stroke Therapy Academic Industry Roundtable (STAIR). Recommendations for standards regarding preclinical neuroprotective and restorative drug development. *Stroke* 1999; 30: 2752–2758.
 33. Finkelstein DM, Schoenfeld DA. Combining mortality and longitudinal measures in clinical trials. *Stat Med* 1999; 18: 1341–1354.
 34. Feuerstein GZ, Zaleska MM, Krams M, et al. Missing steps in the STAIR case: a translational medicine perspective on the development of NXY-059 for treatment of acute ischemic stroke. *J Cereb Blood Flow Metab* 2008; 28: 217–219.
 35. Fisher M, Feuerstein G, Howells DW, et al. Update of the stroke therapy academic industry roundtable preclinical recommendations. *Stroke* 2009; 40: 2244–2250.
 36. Kito G, Nishimura A, Susumu T, et al. Experimental thromboembolic stroke in cynomolgus monkey. *J Neurosci Methods* 2001; 105: 45–53.
 37. Birchenall J, Térémetz M, Roca P, et al. Individual recovery profiles of manual dexterity, and relation to corticospinal lesion load and excitability after stroke—a longitudinal pilot study. *Neurophysiol Clin* 2019; 49: 149–164.
 38. Hillis AE, Baron JC. Editorial: the ischemic penumbra: still the target for stroke therapies? *Front Neurol* 2015; 6: 439–448.
 39. El Amki M, Wegener S. Improving cerebral blood flow after arterial recanalization: a novel therapeutic strategy in stroke. *Int J Mol Sci* 2017; 18: 2669.
 40. Horie N, Morofuji Y, Iki Y, et al. Impact of basal ganglia damage after successful endovascular recanalization for acute ischemic stroke involving lenticulostriate arteries. *J Neurosurg*, Epub ahead of print 31 May 2019. DOI: 10.3171/2019.3.JNS182909
 41. Cho TH, Nighoghossian N, Mikkelsen IK, et al. Reperfusion within 6 hours outperforms recanalization in predicting penumbra salvage, lesion growth, final infarct, and clinical outcome. *Stroke* 2015; 46: 1582–1589.
 42. Ramirez-Garcia G, Harrison KA, Fernandez-Ruiz J, et al. Stroke longitudinal volumetric measures correlate with the behavioral score in non-human primates. *Neuroscience* 2019; 397: 41–55.
 43. Herrmann AM, Meckel S, Gounis MJ, et al. Large animals in neurointerventional research: a systematic review on models, techniques and their application in endovascular procedures for stroke, aneurysms and vascular malformations. *J Cereb Blood Flow Metab* 2019; 39: 375–394.
 44. Zhang Y, Fan F, Zeng G, et al. Temporal analysis of blood–brain barrier disruption and cerebrospinal fluid matrix metalloproteinases in rhesus monkeys subjected to transient ischemic stroke. *J Cereb Blood Flow Metab* 2017; 37: 2963–2974.
 45. Christensen S, Mlynash M, Kemp S, et al. Persistent target mismatch profile >24 hours after stroke onset in DEFUSE 3. *Stroke* 2019; 50: 754–757.
 46. Berkhemer OA, Jansen IGH, Beumer D, et al. Collateral status on baseline computed tomographic angiography and intra-arterial treatment effect in patients with proximal anterior circulation stroke. *Stroke* 2016; 47: 768–776.
 47. Shazeeb MS, King RM, Brooks OW, et al. Infarct evolution in a large animal model of middle cerebral artery occlusion. *Transl Stroke Res*, Epub ahead of print 3 September 2019. DOI: 10.1007/s12975-019-00732-9.
 48. Werner P, Saur D, Zeisig V, et al. Simultaneous PET/MRI in stroke: a case series. *J Cereb Blood Flow Metab* 2015; 35: 1421–1425.
 49. Gottesman RF, Hillis AE. Predictors and assessment of cognitive dysfunction resulting from ischaemic stroke. *Lancet Neurol* 2010; 9: 895–905.
 50. Lee KB, Lim SH, Kim KH, et al. Six-month functional recovery of stroke patients: a multi-time-point study. *Int J Rehabil Res* 2015; 38: 173–180.
 51. Oleksiak A, Postma A, van der Ham IJM, et al. A review of lateralization of spatial functioning in nonhuman primates. *Brain Res Rev* 2011; 67: 56–72.
 52. Payabvash S, Souza LCS, Wang Y, et al. Regional ischemic vulnerability of the brain to hypoperfusion: the need for location specific computed tomography perfusion thresholds in acute stroke patients. *Stroke* 2011; 42: 1255–1260.
 53. Savitz SI, Baron JC, Yenari MA, et al. Reconsidering neuroprotection in the reperfusion era. *Stroke* 2017; 48: 3413–3419.
 54. Savitz SI, Baron JC, Fisher M. Stroke treatment academic industry roundtable X: brain cytoprotection therapies in the reperfusion era. *Stroke* 2019; 50: 1026–1031.